U. Walzer. Systematics of binary intermetallic phases. Phys. Status Solidi (b), 168:397-412, 1991.

Systematics of the Binary Intermetallic Phases

By

U. Walzer

First, a survey is given of semiempirical approaches designed for predicting physical and chemical properties of binary alloy systems from the properties of the elements. The same goal is pursued with the help of a pseudopotential theory with optimum transferability derived from relativistic quantum mechanics. The curves of the *l*-dependent bare-ion pseudopotentials are computed, the spin–orbit coupling being taken into account, and a characteristic radius and a characteristic energy are determined for each of these curves. These dual coordinates are used for the preparation of structure maps in order to predict for binary (1:1) alloys and compounds with a fair degree of probability: space group and structure type of the crystals under normal temperature and pressure conditions, lattice constants, melting temperature, etc. A particularly successful approach is to compute from the dual coordinates a kind of size difference and a function of the hybridization, which then in turn are used as new dual coordinates.

Zuerst wird ein Überblick über die semiempirischen Verfahren gegeben, die für die Vorhersage der physikalischen und chemischen Eigenschaften binärer Legierungen aus den Eigenschaften der Elemente entwickelt wurden. Dasselbe Ziel soll mit Hilfe einer Pseudopotentialtheorie mit optimaler Übertragbarkeit, die aus der relativistischen Quantenmechanik abgeleitet wurde, erreicht werden. Die Verläufe der *l*-abhängigen Ionenpseudopotentiale werden unter Berücksichtigung der Spin–Bahn-Kopplung berechnet und ein charakteristischer Radius sowie eine charakteristische Energie für jede dieser Kurven bestimmt. Diese dualen Koordinaten werden für die Erstellung einer Strukturkarte benutzt, um mit beträchtlicher Wahrscheinlichkeit für binäre (1:1)-Legierungen und -verbindungen die Raumgruppe und den Strukturtyp der Kristalle unter normalen Temperatur- und Druckbedingungen, die Gitterkonstanten, Schmelztemperaturen usw. vorherzusagen. Besonders erfolgreich ist es, aus den dualen Koordinaten eine Art Größendifferenz und eine Funktion der Hybridisierung zu berechnen, die dann als neue duale Koordinaten benutzt werden können.

1. Introduction: Empirical and Semiempirical Methods

It is evident that for practical reasons it is highly desirable to predict from well-known physical properties of the atomic components, the stable crystal structure, the melting temperature, the lattice constants, and other quantities of intermetallic compounds and alloys. On this topic, a survey will be given in the beginning, and then a theoretical proposal will be put forward. Finally, the usefulness of this proposal will be demonstrated by means of illustrations.

In most cases, the afore-mentioned objectives have been implemented through structure maps or similar diagrams. That is, the attempt was made to find two coordinates leading to a more or less pronounced regionalization of the third property in the plot. Kubaschewski [1], for example, used the atomic radius ratio and the cohesive energy ratio for achieving a separation according to the crystal structure. A further attempt in this direction is the heat-of-formation model developed by Miedema [2]. This model makes use of the chemical

potential for the electronic charge, Φ^*, and an empirical quantity, n_{WS}, which later turned out to be the electron density at the boundary of the Wigner-Seitz cell. It is successfully used to the present day as an empirical model [3] although it does not *directly* employ the contributions of the d-electrons to the chemical bonds. In contrast to this, Pettifor's approximation [4] makes direct use of the change in the d-band width and of the centre-of-gravity shift due to alloying.

The use of pseudopotentials for these purposes constituted a significant progress. At first, Simons [5, 6] proposed a simple hard-core form consisting of a Coulomb attraction term describing the attraction between the electron and the ion core and of a quantum defect term. St. John and Bloch [7], proceeding from this approach, introduced as characteristic quantity a radius which is the balance point between the attractive Coulomb force and the repulsive Pauli forces. Since the pseudopotential of a one-valence-electron ion used had been fitted to atomic spectral data, the radii are not physical in a certain sense, but they are nevertheless well suited for preparing the afore-said plots: From differences and sums of these s- and p-radii, an electronegativity difference and an average hybridization were calculated and plotted for 59 octet binary compounds. A separation according to structure types was obtained. Chelikowsky and Phillips [8] extended the table of the afore-mentioned radii to halogens and group-IB metals. Here, too, the bond-orbital σ and π dual coordinates were successfully used for the description of the physical properties. This description was performed for octet binary compounds and suboctet binary compounds with $2 \leqq P \leqq 6$ in separate plots. We shall also partly make use in the present paper of the dual coordinates r_σ and r_π, however, with a completely different calculation of the pseudopotentials. These quantities are calculated from l-dependent ion-core radii r_s^α and r_p^α, with α denoting the atomic species. In the case of a binary compound AB, α thus can be A or B,

$$r_\sigma^\alpha = r_s^\alpha + r_p^\alpha \tag{1}$$

describes s–p σ hybrids, while

$$r_\pi^\alpha = |r_p^\alpha - r_s^\alpha| \tag{2}$$

corresponds to p^2–sp hybrids. The quantity

$$r_\sigma = |r_\sigma^A - r_\sigma^B| \tag{3}$$

is a measure of the total effective core radius difference, whereas

$$r_\pi = r_\pi^A + r_\pi^B \tag{4}$$

indicates the sum of the orbital nonlocality and can be partially considered as a measure of the degree of metallization.

2. First-Principles Approaches

The methods for the systematization of structural properties outlined above can be considerably sophisticated using calculations from first principles directly tackling the all-electron problem. The amount of computation involved is often unreasonably high. Bearing in mind that many low-energy perturbations hardly depend on the almost spherically symmetrical closed-shell core states, the idea is suggested to deal only with the valence states. In this case, the external potential is substituted with a first-principles pseudopotential. Attempts to compensate for the unjustified lowering of the energy of the valence states and

other drawbacks have led to a number of different definitions. For the practical applications intended by us there exist two principal lines of development which are both based on an all-electron single-particle equation for a polyatomic system and the density-functional formalism. In neither approach, fitting of the energy eigenvalues to the experiment is performed. The first principal line obviously was beginning with Zunger and Cohen [9] as well as with Zunger [10]. It is characteristic of this line that the pseudopotential has to satisfy the following conditions: The pseudo-wave functions should be contained in the same core-plus-valence orbital space defined by the spin-density-functional formalism. The pseudo-orbital energies should be equal to the true valence orbital energies. Maximum wave-function similarity within the afore-said orbital subspace is demanded. The Zunger pseudopotential contains the following terms: a non-classical, strongly repulsive, Pauli potential replacing the core–valence orthogonality; an attractive core–valence Coulomb potential; the screened potential generated by the core charge density; a term for the non-linearity of the exchange potential; a term for the non-linearity of the correlation potential; the orthogonality hole potential, and, finally, exchange-correlation potentials generated by the orthogonality hole charge density. After passing from the bare pseudopotential to the ground-state screened atomic pseudopotential, the characteristic radii, one for every angular momentum quantum number l, are determined as the crossing points at which the screened pseudopotential vanishes. These Zunger radii have been employed a number of times in metal chemistry. Villars [11], for example, endeavoured to predict whether or not binary mixtures of elements tend to form a compound. In the second case, he tried to determine whether they are of the solubility type, insolubility type, eutectic type, or peritectic type. To this end, he formed three-dimensional diagrams, one for pairs of elements with the same crystal structure and one for pairs of elements with a different crystal structure. The first dimension of each diagram was a magnitude analogous to (3) but had been computed from Zunger's pseudopotential radii. On the second coordinate, the ratio of the melting temperatures of the two elements was plotted in K, with the greater number being given in the numerator. The third coordinate constituted the difference between the number of valence electrons. Villars succeeded in obtaining a good separation of the different types. In [12], this attempt was transferred to ternary alloy systems, the listed magnitudes of the element pairs being substituted with the arithmetic mean of these magnitudes of three element pairs each.

Andreoni et al. [13, 14] examined the equilibrium shapes of sp-bonded nonhydride AB_2 molecules. They were particularly interested in determining whether the molecule is linear or bent and in the size of the apex angle. The Zunger size difference r_σ and the dual Zunger quantity r_π, which is a function of the hybridization, on the one hand, and a nodal radius scheme [15], on the other hand, were used for preparing the structural plots. This classification was also applied to AB_3 and A_2B_2 compounds [16].

Using structural plots, we want to predict in this paper quantities other than the afore-mentioned ones. Moreover, our approach is based on the other principal line of development for first-principles pseudopotentials which started with Hamann et al. [17] and was continued by Bachelet et al. [18, 19] and by Greenside and Schlüter [20]. We developed the theory further and wrote completely new computer programs.

3. Theory

Since heavier atoms are affected by spin–orbit effects, we use the Dirac equation as starting point. In the case of a central potential $V(r)$, this linear matrix equation with partial

first-order derivatives is reduced to the following two coupled differential equations:

$$\frac{dG_i(r)}{dr} + \frac{\varkappa}{r} G_i(r) - [2\alpha^{-2} + \varepsilon_i - V(r)]\,\alpha F_i(r) = 0\,, \tag{5}$$

$$\frac{dF_i(r)}{dr} - \frac{\varkappa}{r} F_i(r) + [\varepsilon_i - V(r)]\,\alpha G_i(r) = 0\,. \tag{6}$$

The electronic charge density is obtained through the summation over the occupied states i,

$$\varrho(r) = \sum_{i=1}^{N} [|F_i(r)|^2 + |G_i(r)|^2]\,. \tag{7}$$

We use exclusively atomic units, thus,

$$\hbar = m = e = 1 \quad \text{and} \quad c = \alpha^{-1} = 137.037\,.$$

The relativistic quantum number $\varkappa$ is obtained from the angular momentum quantum number l,

$$\varkappa = -(l+1) \quad \text{for} \quad j = l + 1/2 \quad \text{and} \quad \varkappa = l \quad \text{for} \quad j = l - 1/2\,.$$

Neglecting higher-order terms, the following differential equation for the determination of the major wave-function component $G_\varkappa(r)$ follows from (5) and (6):

$$\frac{1}{2}\left(\frac{d^2G_\varkappa}{dr^2} - \frac{\varkappa(\varkappa+1)}{r^2} G_\varkappa\right) - (V(r) - \varepsilon)\,G_\varkappa = 0\,. \tag{8}$$

From this equation, thus, the pseudo-wave functions and pseudopotentials are derived, the following fundamental requirements having been satisfied:

a) Outside the core radius r_c true and pseudo atomic wave functions are in agreement.

b) For a certain atomic configuration, the real and pseudo valence eigenvalues are identical.

c) For each valence state, the integrals from 0 to r of the real and pseudo charge densities are in agreement if $r > r_c$. As a result, the electrostatic potential outside the core radius is in conformity for real and pseudo electronic charge distributions.

d) For $r > r_c$, the logarithmic derivatives of the true and pseudo wave functions are in conformity. This is also true for the first energy derivatives.

This last condition effects that the scattering properties of the real ion cores are fairly well described. Transferability is achieved through the last *two* conditions, i.e. the pseudopotentials can be used for both atoms and molecules, clusters, solids, and surfaces. The ground state energy of the electrons was computed by means of the local-density-functional approach [21] and is made up of the following constituent parts: kinetic energy of the non-interacting electrons, Coulomb energy of the electrons, nuclear potential, and exchange-correlation energy. Interpolation formulas [22, 23] were required only for the last term. With respect to these formulas, too, relativistic quantum-electrodynamical corrections were applied. All these expressions can be computed from the charge density.

The bare-ion pseudopotentials were computed in five stages:

a) $G_\varkappa$ was computed from (8). It yielded $F_\varkappa$ and a set of one-electron eigenvalues.

b) In the screened full-core potential, the singularity is cut off at $r = 0$.

c) This is followed by a normalization.

d) Inverting the radial Schrödinger-type equation yields the final screened pseudo potentials.

e) Eventually, these final screened pseudopotentials are unscreened.

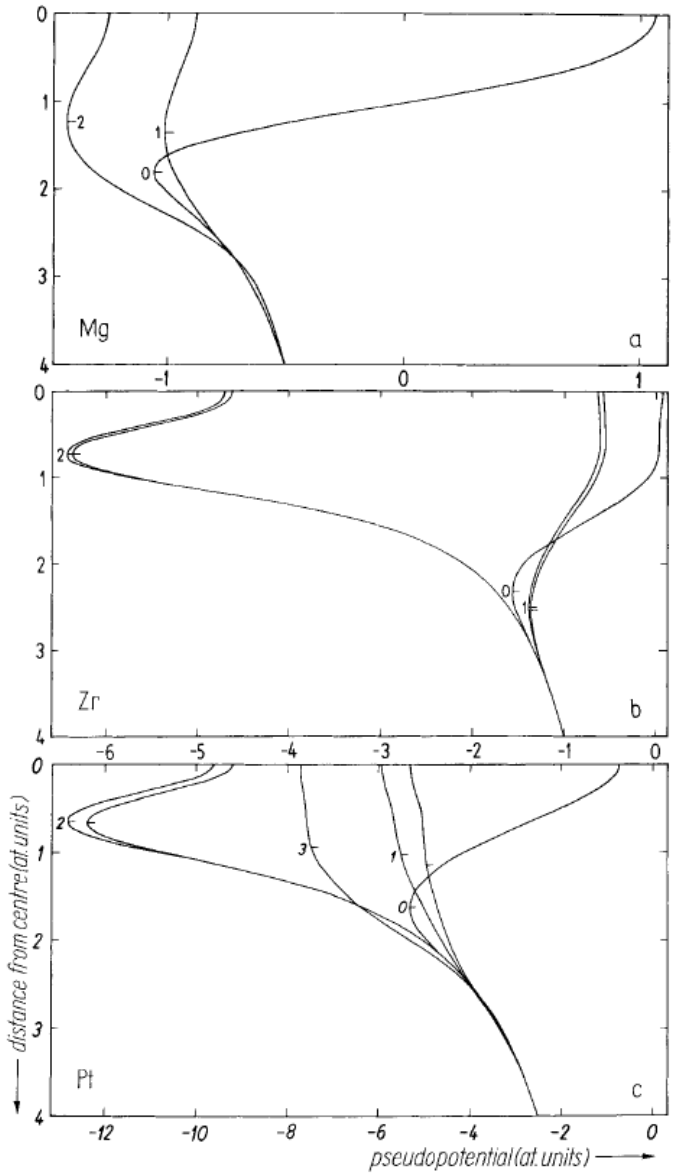

Fig. 1. Pseudopotential for a) Mg, b) Zr, and c) Pt. The distance from the centre of the atom has been plotted downwards, and the ion-core pseudopotential towards the right, both in at. units. The angular momentum quantum number l is given on the pertaining curve. Minima or maximum curvature locations (for more details, see text) have been designated by short dashes at the curves

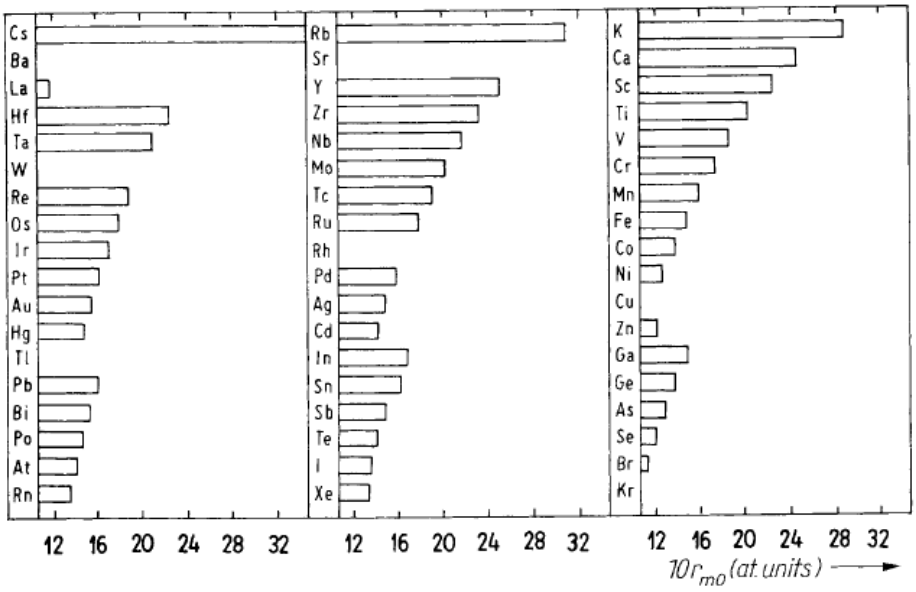

Fig. 2. Radius r_{mo}, represented in the Periodic Table

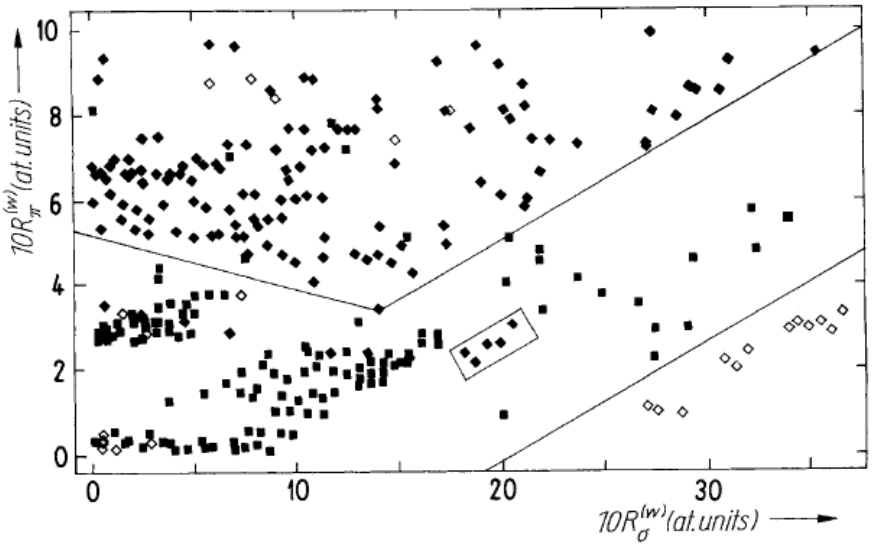

Fig. 3. Crystal lattices as a function of $R_{\sigma}^{(w)}$ and $R_{\pi}^{(w)}$

A detailed description of the computations will be published elsewhere [24]. Fig. 1a to c show some of the computed pseudopotentials as a function of the distance r from the centre of the atom. The numbers on the curves denote the pertaining angular momentum quantum numbers l. The curves are split through spin–orbit effects. However, this becomes visible only for the heavier elements of which zirconium and platinum were shown by us as examples. For each curve, one characteristic point was determined with the help of the following procedure: For the case that the pseudopotential v has its smallest value in the centre of the atom, we take the genuineness e to be zero. Otherwise, $e = 1$. For $e = 0$, the characteristic number pair r, v is located at the point of the curve where $d^2v/dr^2 > 0$ and where the curvature k, coming from the infinitely large distance r, reaches a maximum for the first time. We have

$$k = \frac{d^2v}{dr^2}\left[1 + \left(\frac{dv}{dr}\right)^2\right]^{-3/2}. \tag{9}$$

For $e = 1$, the characteristic number pair r, v represents the first minimum of the curve, coming from the side of infinite distance r. In this way, the following quantities were determined for the chemical elements:

$$\begin{aligned} &r_{m0}, v_{m0}, e_{m0}; r_{m1}, v_{m1}, e_{m1}; r_{p1}, v_{p1}, e_{p1}; \\ &r_{m2}, v_{m2}, e_{m2}; r_{p2}, v_{p2}, e_{p2}; r_{m3}, v_{m3}, e_{m3}. \end{aligned} \tag{10}$$

Each of these number triples separated by a semicolon represents a characteristic point: distance from the centre of the atom, pseudopotential, and genuineness. The first index, i.e., m or p, denotes the spin state. The second index is the angular momentum quantum number. In the description given in the following section, a further index which is a label for the atom type has been attached. Thus, in a binary mixture, it may be 1 or 2.

4. Graphic Representation of the Results

All theoretical numerical values represented in the plots have been computed by means of the theory outlined above; all experimental data come from the handbook by Villars and Calvert [25]. To exclude any subjective aspects from the discussion, no values were eliminated. All characteristic radii have a systematic distribution in the Periodic Table. A kind of s-state radius, namely r_{m0}, is shown as an example in Fig. 2. In analogy to (3) and (4) and using (10), we now define the size difference $R_\sigma^{(w)}$ and a function of the hybridization $R_\pi^{(w)}$,

$$R_\sigma^{(w)} = |(r_{11} + r_{m01}) - (r_{12} + r_{m02})|, \tag{11}$$

where $r_{11} = (r_{m11} + r_{p11})/2$ and $r_{12} = (r_{m12} + r_{p12})/2$, and

$$R_\pi^{(w)} = |r_{11} - r_{m01}| + |r_{12} - r_{m02}|. \tag{12}$$

Fig. 3 shows $R_\pi^{(w)}$ versus $R_\sigma^{(w)}$. The symbols denote the space group and structure type of the crystal (see Table 1). A distinct separation of the three depicted lattices can be noted: Solid diamonds represent lattices with the space group $Pm\bar{3}m$ and structure type ClCs, solid squares the space group $Fm\bar{3}m$ and structure type ClNa, open diamonds the space group $P6_3/mmc$ and structure type Mg. This means that, if a compound or alloy with a certain lattice from the three is to be produced, quite good predictions can be made, or a

Table 1
Symbol assignment in the diagrams in which the symbols designate the space group of the crystal lattice

space group	structure type	symbol	description of symbol
$Fm\bar{3}m$	ClNa	■	solid square
$Fm\bar{3}m$	Cu	□	open square
$F\bar{4}3m$	SZn	○	open circle
$Fd\bar{3}m$	NaTl	∧	right angle, tip pointing upwards
$Pm\bar{3}m$	ClCs	◆	solid diamond
$P6_3/mmc$	AsNi	●	solid circle
$P6_3/mmc$	Mg	◇	open diamond
$P6_3mc$	SZn	∨	right angle, tip pointing downwards
Pnma	BFe	▼	solid triangle, tip pointing downwards
Pnma	MnP	▲	solid triangle, tip pointing upwards
P4/mmm	AuCu	◀	solid triangle, tip pointing to the left
P4/nmm	CuTi	▶	solid triangle, tip pointing to the right
$P\bar{4}3n$	GeK	<	right angle, tip pointing to the left
$P2_13$	FeSi	>	right angle, tip pointing to the right
Cmcm	BCr	+	upright cross
$Im\bar{3}m$	W	×	canted cross
$I4_1/acd$	NaPb	*	canted cross with additional horizontal beam

lot of experimental work is superfluous since the coordinates can simply be computed by means of the pseudopotential theory.

$R_\pi^{(w)}$ is, to a certain extent, a measure of the sum of the orbital nonlocality of the s and p electrons. $R_\sigma^{(w)}$ is, however, the difference of the sums of the core radii for $l = 0$ and 1, which have been computed by means of the bare-ion pseudopotentials. A rough interpretation of the coordinates used in Fig. 3 is as follows: $R_\pi^{(w)}$ corresponds to p^2–sp hybrids, however, $R_\sigma^{(w)}$ corresponds to s–p σ hybrids. We did not use the discrimination between octet compounds and nonoctet compounds because the assignment of a compound is sometimes arbitrary. If we drop the doubtful cases and use the octet–nonoctet discrimination, then the topological separation will be even more distinct. If we construct a similar plot by means of Miedema parameters [2, 3], then we receive no separation. In the Miedema diagram, the difference of the third roots of the electronic density at the Wigner-Seitz cell boundary is plotted towards the right, the difference in the effective elemental work functions is plotted on the ordinate.

In Fig. 4, an averaged pseudopotential has been plotted versus an averaged radius for $l = 1$. Only materials with space group $Fm\bar{3}m$ and structure type ClNa were taken. Moreover, we have confined ourselves to compounds and alloys of a transition metal and a simple metal. The symbols denote intervals of the lattice constant a (in 10^{-10} m) with

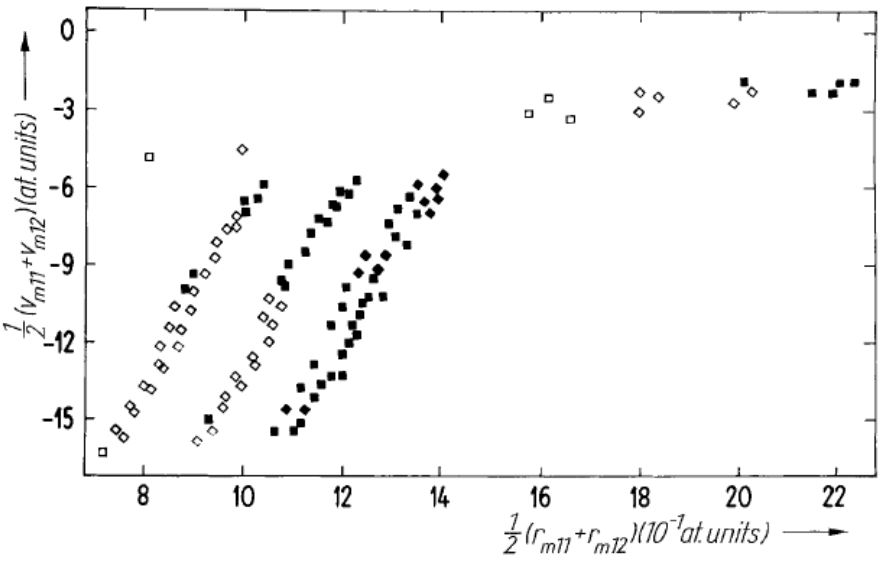

Fig. 4. Radius–potential diagram for $l = 1$

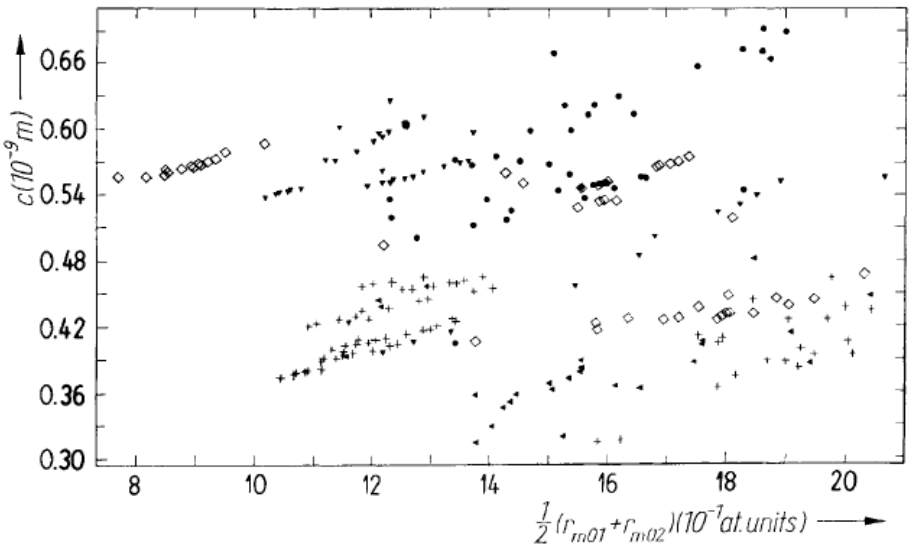

Fig. 5. Radius–lattice constant diagram. The symbols denote the space group and structure type of the crystals. Table 1 gives the meaning of the symbols

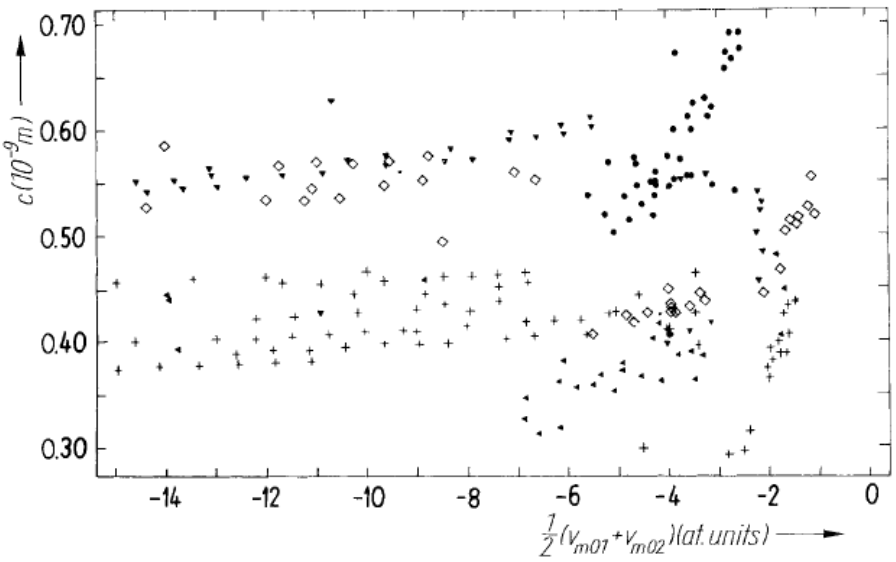

Fig. 6. Potential–lattice constant diagram. The symbols denote the space group and structure type of the crystals (see Table 1)

solid diamonds $a \geqq 6.3665$,
solid squares $6.3665 > a \geqq 5.8517$,
open diamonds $5.8517 > a \geqq 5.3369$,
open squares $5.3369 > a \geqq 4.8221$.

Not just the regular pattern is of interest, but also the fact that, using this diagram, one can predict the size class of the lattice constant a. In Fig. 5, the lattice constant c has been plotted versus an averaged radius for $l = 0$. The symbols denote the different lattices. Here, too, the lattice types are by no means randomly distributed, but in certain parts of the plot points of the same lattice accumulate.

If the lattice constant c is plotted versus the averaged pseudopotential for $l = 0$ (see Fig. 6), the separation according to space group and structure type is even more pronounced than in the previous diagram. We define a function F as follows:

$$F = [(C - 1)/(18 - 1)]\,(r_{m0} - 1)\,v_{m0}\,,$$

where C is the number of the column in the Periodic Table containing the element. For AB compounds and alloys of two transition metals, the melting temperature T_m increases with the mean value of F. The quantities r_{m0} and v_{m0} are given in atomic units. In Fig. 7, $\bar{F}$ has been plotted versus the melting temperature. Solid diamonds represent the compounds and alloys of two transition metals (TT), crosses those of two simple metals (SS), and open diamonds represent the compounds and alloys of a transition metal and a simple metal (ST). In particular for high temperatures we can see a distinct separation of the three point

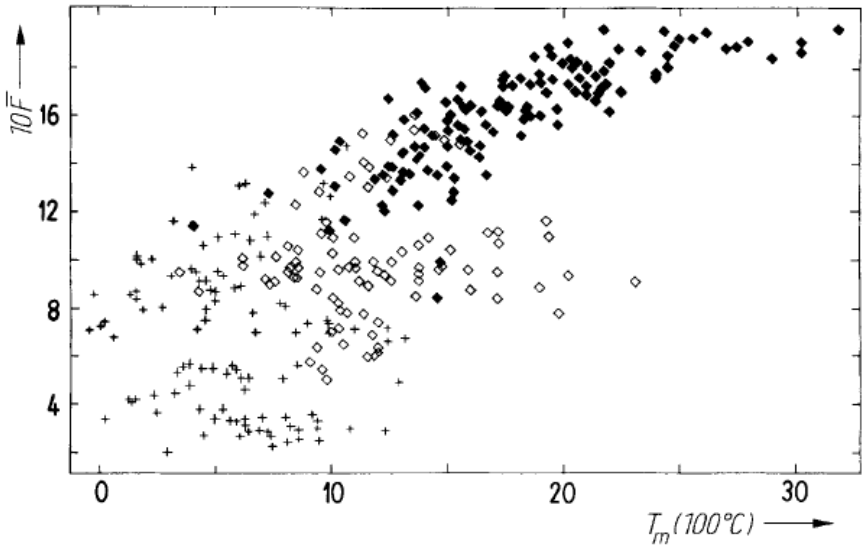

Fig. 7. T_m–$\bar{F}$ diagram. T_m is the melting temperature. $\bar{F}$ is the mean value of the function F

clusters. The separation into three point clouds and the linear $\bar{F}$ increase of the TT points versus the temperature of fusion T_m mean a progress in predictability. Efforts to predict the melting temperature by means of the atomic radii, atomic numbers, electronegativity,

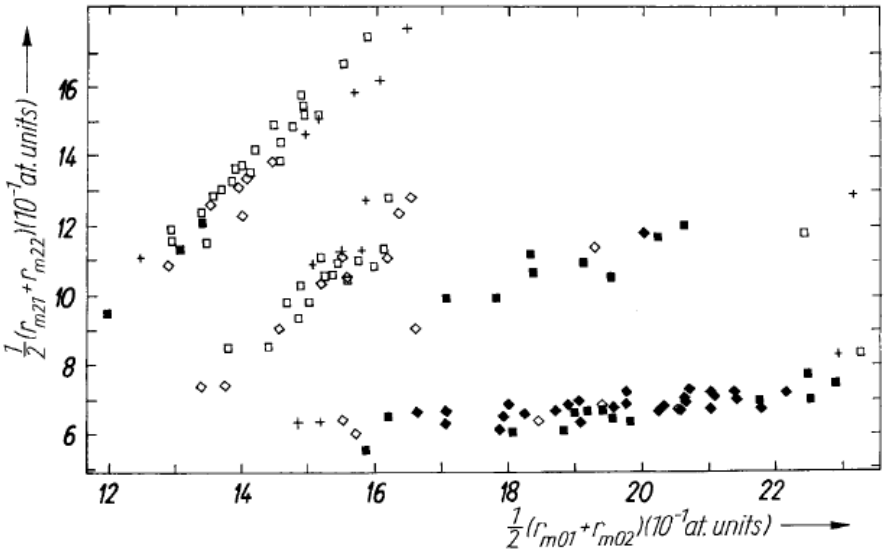

Fig. 8. Radius–radius diagram

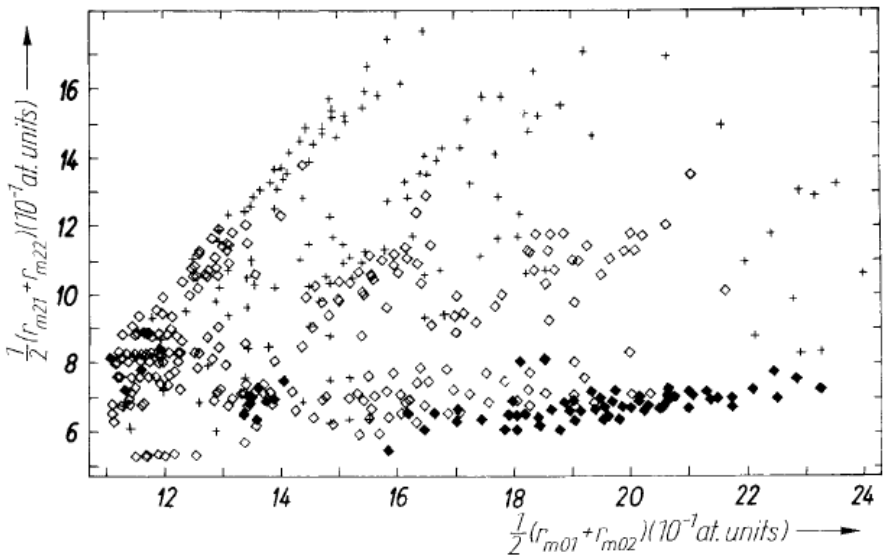

Fig. 9. Radius–radius diagram. Solid diamonds denote TT, open diamonds ST, and crosses SS (see also text for Fig. 7)

and number of valence electrons have been only of limited success. Only the use of the elemental melting points results in similar elongated point clouds of the TT points [26] and of the ST points. The predictability by means of the SS point cloud is low.

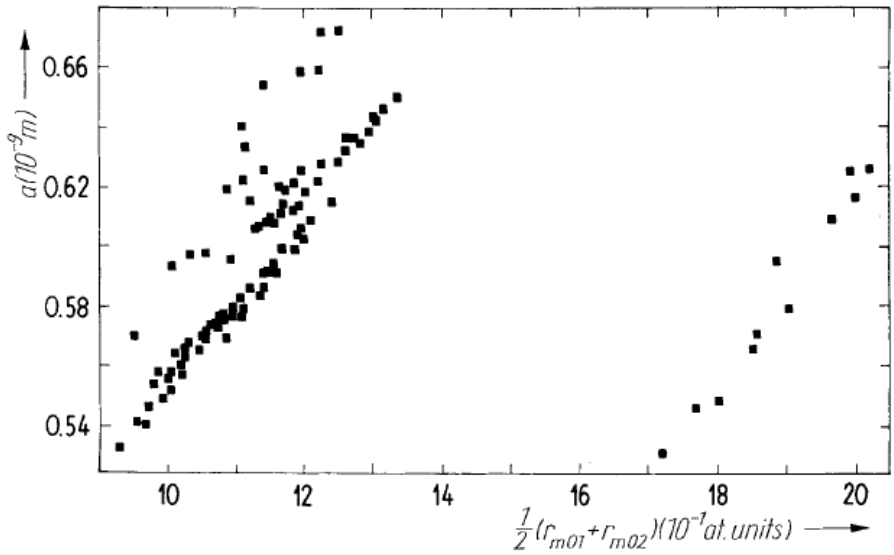

Fig. 10. Radius–lattice constant diagram

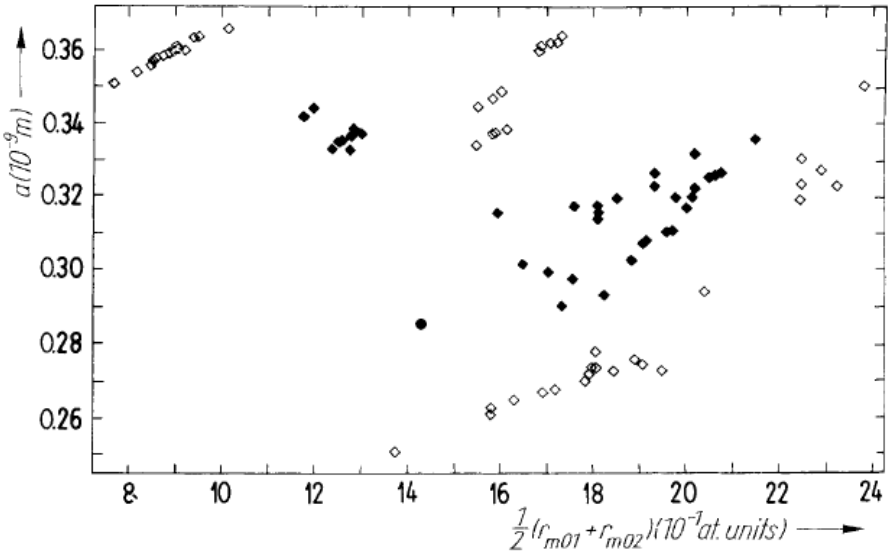

Fig. 11. Radius–lattice constant diagram

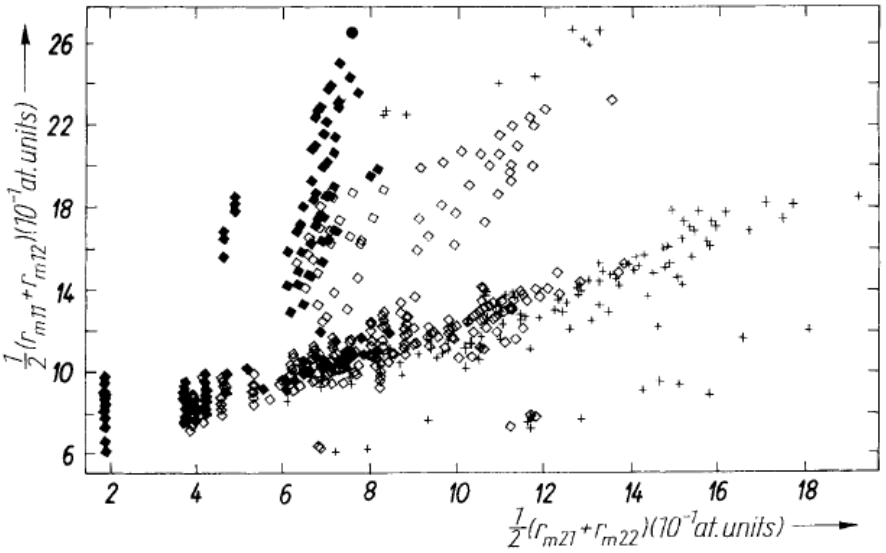

Fig. 12. Radius–radius diagram

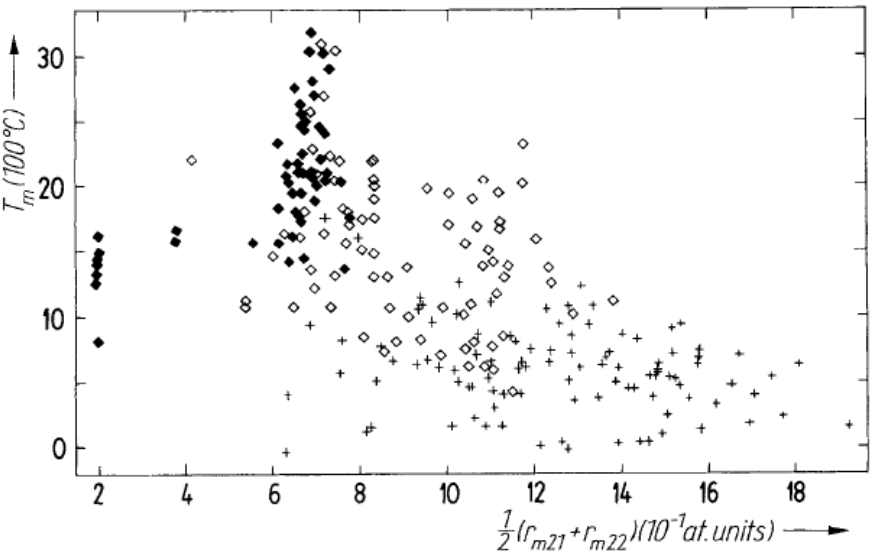

Fig. 13. Radius–melting temperature diagram. Solid diamonds represent TT, open diamonds ST, crosses SS

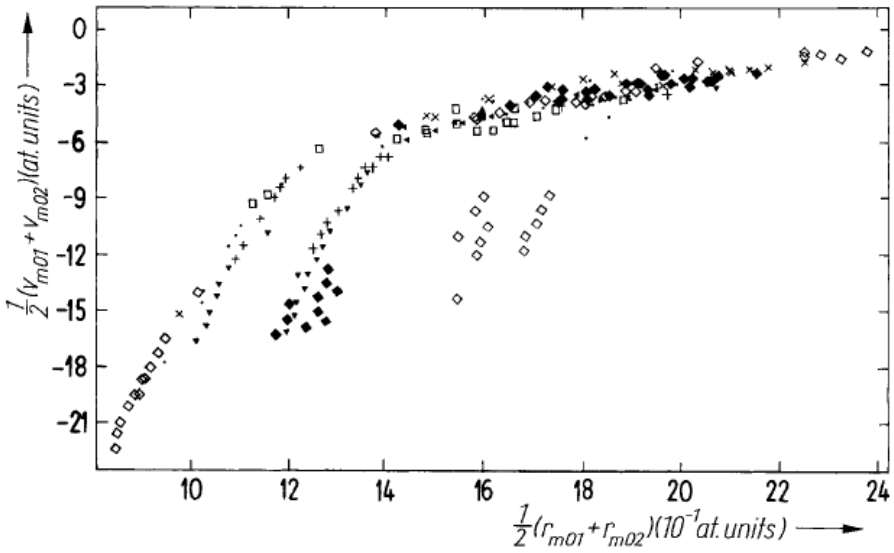

Fig. 14. Radius–potential diagram for $l = 0$. The symbols denote the space group and structure type of the lattice. For details, see Table 1

In Fig. 8, the mean value of the radii for $l = 2$ has been plotted versus the mean of the radii for $l = 0$. Only binary (1:1) mixtures of the elements of the fourth, fifth, and sixth periods without rare-earth elements were taken. The symbols represent intervals of the melting temperature T_m (in °C) with

solid diamonds	$T_m \geqq 2028$,
solid squares	$2028 > T_m \geqq 1487$,
open diamonds	$1487 > T_m \geqq 946$,
open squares	$946 > T_m \geqq 405$,
crosses	$405 > T_m$.

Not only the separation of the symbols into four elongated clusters is noteworthy here, but also the possibility to predict the melting point class. In Fig. 9, the mean value of the radii of the characteristic points for $l = 2$ has been plotted versus the mean radii of the characteristic points for $l = 0$. Only a slight dependence on the mean value of the d-state radii is found for alloys and intermetallic compounds of two transition metals (TT) which have been plotted here as solid diamonds. The plot in Fig. 10 shows the lattice constant a versus the mean radii for $l = 0$. Only compounds and alloys of a simple metal and a transition metal whose lattice corresponds to the space group $Fm\bar{3}m$ and structure type ClNa have been used. A radius–lattice constant diagram can be seen in Fig. 11. Only compounds and alloys of two transition metals are plotted. Solid diamonds represent space group $Pm\bar{3}m$ and structure type ClCs, open diamonds $P6_3/mmc$ and structure type Mg. Also in this case the lattice types are distinctly separated into different areas. An advantage of the present method of best separation is the uniform derivation of the two coordinates used. Both characteristic pseudopotential and characteristic radius stem from a unified approach which has been derived from quantum mechanics. Previous separation approaches often use a mixture of experimental and theoretical quantities. For example, Villars [11] received the best results using three coordinates: the difference between the numbers of valence electrons, the absolute difference between the Zunger radius sums, and the ratio of the melting temperatures of the two elements, the higher magnitude being the numerator.

Fig. 12 shows the mean value of the characteristic radii for $l = 1$ versus the average of the radii for $l = 2$. Solid diamonds represent TT, open diamonds ST, and crosses SS. Apart from an area with mean radii, a distinct separation of the three point clusters can be noted. The dependence of the melting temperature on the mean value of the d-state radii is given in Fig. 13, while Fig. 14 shows a typical dependence of the potential (ordinate) on the radius, in this case especially for $l = 0$. Points of an identical lattice structure are located on special curve sections or in small areas.

5. Conclusions

From a pseudopotential theory with optimum transferability, a potential curve has been computed as a function of the radius for each chemical element, for each angular momentum quantum number, and for each spin state. The information contained in these curves has been somewhat condensed into a characteristic point. These dual coordinates and simple functions of them served for the preparation of structure maps and similar diagrams which do not just permit to predict the crystal structure, but also the melting temperature, lattice constants, etc. Thus, if we want to create a binary alloy or an intermetallic compound with a certain desired property, we can see from the diagrams prior to the experiment whether

this attempt is promising. The characteristic bare-ion pseudopotential radii can be used with good success in order to systematize the chemical and structural properties of binary AB systems. They can be used to compute the major orbital contributions to binding energies.

References

[1] O. KUBASCHEWSKI, in: The Physical Chemistry of Metallic Solutions and Intermetallic Compounds, Vol. 1, Chemical Publ. Co., New York 1960.
[2] A. R. MIEDEMA, R. BOOM, and F. R. DE BOER, in: Crystal Structure and Chemical Bonding in Inorganic Chemistry, Ed. C. J. M. ROOYMANS and A. RABENAU, North-Holland Publ. Co., Amsterdam 1975.
[3] F. R. DE BOER, R. BOOM, W. C. M. MATTENS, A. R. MIEDEMA, and A. K. NIESSEN, Cohesion in Metals–Transition Metal Alloys, North-Holland Publ. Co., Amsterdam 1988.
[4] D. G. PETTIFOR, Phys. Rev. Letters **42**, 846 (1979).
[5] G. SIMONS, J. chem. Phys. **55**, 756 (1971).
[6] G. SIMONS, Chem. Phys. Letters **12**, 404 (1971).
[7] J. ST. JOHN and A. N. BLOCH, Phys. Rev. Letters **33**, 1095 (1974).
[8] J. R. CHELIKOWSKY and J. C. PHILLIPS, Phys. Rev. B **17**, 2453 (1978).
[9] A. ZUNGER and M. L. COHEN, Phys. Rev. Letters **41**, 53 (1978).
[10] A. ZUNGER, A Pseudopotential Viewpoint of the Electronic and Structural Properties of Crystals, in: M. O'KEEFFE and A. NAVROTSKY (Ed.), Structure and Bonding in Crystals, Vol. I, Academic Press, New York 1981 (pp. 73 to 135).
[11] P. VILLARS, J. less-common Metals **109**, 93 (1985).
[12] P. VILLARS, J. less-common Metals **119**, 175 (1986).
[13] W. ANDREONI, G. GALLI, and M. TOSI, Phys. Rev. Letters **55**, 1734 (1985).
[14] W. ANDREONI and G. GALLI, Phys. Chem. Minerals **14**, 389 (1987).
[15] W. ANDREONI, Helv. Phys. Acta **58**, 226 (1985).
[16] W. ANDREONI and G. GALLI, Phys. Rev. Letters **58**, 2742 (1987).
[17] D. R. HAMANN, M. SCHLÜTER, and C. CHIANG, Phys. Rev. Letters **43**, 1494 (1979).
[18] G. B. BACHELET, G. A. BARAFF, and M. SCHLÜTER, Phys. Rev. B **24**, 4736 (1981).
[19] G. B. BACHELET, D. R. HAMANN, and M. SCHLÜTER, Phys. Rev. B **26**, 4199 (1982).
[20] H. S. GREENSIDE and M. SCHLÜTER, Phys. Rev. B **28**, 535 (1983).
[21] W. KOHN and L. J. SHAM, Phys. Rev. **140**, A1133 (1965).
[22] D. M. CEPERLEY and B. J. ALDER, Phys. Rev. Letters **45**, 566 (1980).
[23] J. PERDEW and A. ZUNGER, Phys. Rev. B **23**, 5048 (1981).
[24] U. WALZER, The Application of a Pseudopotential Approach to the Physics of Binary Intermetallic Compounds, High Temp. – High Pressures, to be published.
[25] P. VILLARS and L. D. CALVERT, Pearson's Hdb. of Crystallographic Data for Intermetallic Phases, Vol. 1 to 3, Amer. Soc. Metals, Metals Park, Ohio 1985.
[26] J. R. CHELIKOWSKY and K. E. ANDERSON, J. Phys. Chem. Solids **48**, 197 (1987).

(Received May 21, 1991; in revised form August 19, 1991)